ORIGINAL PAPER

Intrinsic and Extrinsic Temperature-Dependency of Viscosity-Sensitive Fluorescent Molecular Rotors

**Sarah Howell · Marianna Dakanali ·
Emmanuel A. Theodorakis · Mark A. Haidekker**

Abstract Molecular rotors are a group of environment-sensitive fluorescent probes whose quantum yield depends on the ability to form twisted intramolecular charge-transfer (TICT) states. TICT formation is dominantly governed by the solvent's microviscosity, but polarity and the ability of the solvent to form hydrogen bonds play an additional role. The relationship between quantum yield ϕ_F and viscosity η is widely accepted as a power-law, $\phi_F = C \cdot \eta^x$. In this study, we isolated the direct influence of the temperature on the TICT formation rate by examining several molecular rotors in protic and aprotic solvents over a range of temperatures. Each solvent's viscosity was determined as a function of temperature and used in the above power-law to determine how the proportionality constant C varies with temperature. We found that the power-law relationship fully explains the variations of the measured steady-state intensity by temperature-induced variations of the solvent viscosity, and C can be assumed to be temperature-independent. The exponent x, however, was found to be significantly higher in aprotic solvents than in protic solvents. We conclude that the ability of the solvent to form hydrogen bonds has a major influence on the relationship between viscosity and quantum yield. To use molecular rotors for the quantitative determination of viscosity or microviscosity, the exponent x needs to be determined for each dye-solvent combination.

Keywords Molecular rotors · Viscosity sensors · Twisted intramolecular charge transfer · TICT · Polarity · Hydrogen bonds

Introduction

Molecular rotors are fluorescent environment-sensitive molecules with strong dependency of their emission spectra on the polarity and viscosity of the environment [1–4]. The photophysical principle of molecular rotors is based on their ability to form twisted intramolecular charge transfer (TICT) complexes: Upon photoexcitation, an electron is transferred from an electron donor group to an electron acceptor group within the same molecule. Under the ensuing electrostatic force, the molecule has a high propensity to assume a twisted state with a lower excited-state/ground-state energy gap [5, 6]. The energy gap can be so small that relaxation from the TICT state occurs without photon emission, and emission occurs from the planar, locally excited (LE) state with a high sensitivity of the quantum yield towards the viscosity of the solvent, but a low sensitivity towards polarity [6–8].

These molecules enjoy growing popularity as real-time microviscosity probes [4, 7, 9–13], because their quantum yield increases with the viscosity of the solvent. The relationship between a molecular rotor's quantum yield ϕ_F and the solvent viscosity η is most

S. Howell · M. A. Haidekker (✉)
Faculty of Engineering, University of Georgia,
597 D.W. Brooks Drive, Athens, GA 30602, USA
e-mail: mhaidekk@uga.edu

M. Dakanali · E. A. Theodorakis
Department of Chemistry and Biochemistry,
University of California, San Diego, 9500 Gilman Drive,
La Jolla, CA 92093, USA

commonly described by a power-law, often referred to as the Förster–Hoffmann equation (Eq. 1):

$$\phi_F = C \cdot \left(\frac{\eta}{\sigma}\right)^x \qquad (1)$$

where C is a dye-dependent constant, x is both dye-and solvent-dependent, and σ is a dye-dependent constant that reflects the mechanical and electrostatic properties of the rotating group and has units of viscosity [14]. Förster and Hoffmann [14] derived this equation under the assumption that the twisting molecular segments experience microfriction that is linked to the bulk viscosity through the Debye–Stokes–Einstein (DSE) model of viscosity, whereas Loutfy et al. [15] arrived at the same power-law relationship by assuming that diffusion is primarily governed by molecular free volume. An in-depth review of the theory underlying Eq. 1 can be found in [16]. Equation 1 is often found in the literature in its logarithmic form, with C and σ^{-x} combined into one single constant:

$$\log \phi_F = C + x \cdot \log \eta \qquad (2)$$

In the rigorous derivation by Förster and Hoffmann, the constant C is determined by the physical properties of the dye, such as the excited-state electrostatic forces and the difference between the lowest-energy intramolecular rotation angle in the ground- and excited states, whereby $x \equiv 2/3$ as result of an integration step. In the empirical derivation by Loutfy et al., the constant C depends on both the dye and the solvent, and the exponent x was experimentally determined [2] and found to be near 0.6 [1, 7, 10, 17]. Some studies stipulate a temperature-dependent rate of TICT formation [1, 3, 18], where the relaxation rate through intramolecular rotation (i.e., TICT formation), k_{rot}, follows an Arrhenius function (Eq. 3),

$$k_{rot} = k_{rot}^0 \cdot \exp\left(-\frac{E_A}{k_B T}\right) \qquad (3)$$

where k_{rot}^0 is an intrinsic, dye-dependent reorientation rate, E_A is an apparent activation energy, k_B is Boltzmann's constant, and T the temperature. The quantum yield ϕ_F is inversely proportional to k_{rot}, and therefore, temperature can be assumed to have a significant direct effect on the fluorophore's quantum yield. The assumption of a temperature-dependent behavior is reasonable, because the quantum yield of most fluorescent molecules decreases with increasing temperature, but the exact temperature-dependent reorientation rate is difficult to determine, because temperature-dependent viscosity changes also influence the reorientation (i.e. TICT formation) rate. To our knowledge, the temperature-dependent behav-

ior of the constants C and x in Eq. 1 has not been fully examined.

When molecular rotors are applied to determine viscosity, either in bulk fluids [19] or in spatially-resolved viscosity maps [13, 20, 21], the question of an intrinsic temperature dependency becomes crucial, because the viscosity of fluids itself is temperature-dependent. Therefore, the goal of this study is to examine C and x as functions of temperature by accounting for temperature-dependent viscosity changes in the solvent. We found that the quantum yield change is explained by the temperature-dependent change in solvent viscosity, and temperature-dependent changes of C and x have negligible influence on the quantum yield.

Materials and methods

Theoretical approach

In steady-state spectroscopy, emission intensity I_{em} is proportional to the quantum yield ϕ_F of a fluorophore, to instrument gain factors g, to excitation intensity I_{ex}, and—for low dye concentrations—to the dye concentration c,

$$I_{em} = g \cdot c \cdot I_{ex} \cdot \phi_F \qquad (4)$$

We now combined the temperature-independent extrinsic factors into one constant G and substituted the quantum yield with the viscosity-dependent term from Eq. 1. However, we allowed x to be a variable parameter instead of setting $x \equiv 2/3$ as required by Förster and Hoffmann. Under these assumptions, Eq. 4 can be rewritten as

$$I_{em}(T) = G \cdot \hat{C}(T) \cdot \eta(T)^x \qquad (5)$$

where (T) indicates a function of temperature. In relation to Eq. 1, we use $\hat{C} = C \cdot \sigma^{-x}$ to combine the specific dye-dependent factors that govern intramolecular rotation, and we refer to $\hat{C}$ as the *intrinsic quantum yield* of the dye as it is a proportionality factor for the quantum yield. Under the assumption of a temperature-driven reorientation rate (Eq. 3), $\hat{C}$ will exhibit temperature-dependent behavior.

To isolate $\hat{C}(T)$, we determined the temperature-dependency of the solvent viscosity, $\eta(T)$, and acquired emission intensities $I_{em}(T)$ in the same temperature range. To reduce experimental error caused by the viscosity measurement, we assumed all solvents to follow the Vogel–Fulcher–Tammann model, Eq. 6,

$$\eta(T) = \eta_0 \cdot \exp\left(\frac{v_g}{v_g + \alpha(T - T_g)}\right) \qquad (6)$$

where η_0 is a proportionality constant, v_g is the volume at the glass-transition temperature, α is the linear thermal expansion coefficient, and T_g is the glass transition temperature. The Vogel–Fulcher–Tammann model has been named after the authors of individual works [22–24] and is widely used to describe the temperature-dependent viscosity behavior of glass-forming liquids, which includes the solvents used in this study (see e.g., [25, 26] for an overview). Instead of using individual measurements of the viscosity at a specific temperature T, we determined the constants in Eq. 6 from the entire temperature series through nonlinear regression and used the viscosity from Eq. 6, thus reducing point-to-point errors.

We assumed the constant G in Eq. 5 to be temperature-independent and defined a new variable $\zeta(T)$ that is proportional to both the constant G and the temperature-dependent intrinsic component of the fluorophore, $\hat{C}$:

$$\zeta(T) = G \cdot \hat{C}(T) \tag{7}$$

The new variable $\zeta(T)$, which we refer to as *intrinsic intensity* to distinguish it from the intrinsic quantum yield $\hat{C}(T)$, captures the temperature-dependent behavior of the fluorophore, and at the same time becomes measurable with steady-state fluorescence when Eq. 7 is substituted into Eq. 5, which is then solved for $\zeta(T)$:

$$\zeta(T) = \frac{I_{em}(T)}{\eta(T)^x} \tag{8}$$

We then calculated $\zeta(T)$ from the measured data points of viscosity and emission intensity at a specific temperature, plotted $\zeta(T)$ over the temperature T and examined the plot for any trends. If the hypothesis of a temperature-driven reorientation rate is correct, a consistent decline of $\zeta(T)$ with increasing temperature must be found. More specifically, if the intramolecular rotation rate follows an Arrhenius-type behavior, we expect to find a good nonlinear curve fit of Eq. 3 into the data points of $\zeta(T)$ over T.

Materials

Eight solvents were used, covering both polar protic and polar aprotic groups. The polar protic solvents were isopropanol, ethylene glycol, ethanol, and pentanol. The polar aprotic solvents included dimethyl sulfoxide (DMSO), dimethylformamide (DMF), propylene carbonate, and *n*-methyl-2-pyrrolidone (NMP). All solvents were spectroscopy-grade and purchased from Sigma-Aldrich (St. Louis, MO). Six molecular rotors, whose structures can be seen in Fig. 1, were
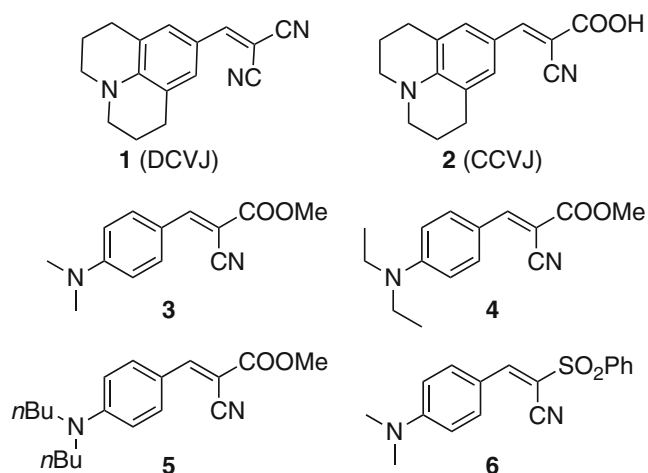

Fig. 1 Chemical structures of the molecular rotors used in this study. **1** and **2** are the commercially available DCVJ and CCVJ, respectively. **3**–**5** are a family of anilino-based molecular rotors with increasing chain length at the donor group, and **6** is similar to **3**, but with a phenyl-sulfonyl group replacing the ester group

used with each solvent independently. Molecular rotors **1** and **2** are 9-(2,2-dicyanovinyl)julolidine (DCVJ) and 9-(2-carboxy-2-cyanovinyl)julolidine (CCVJ), respectively, and were purchased from Invitrogen. Molecular rotors **3** through **5** are a related family of p-N, N-dialkylaminobenzylidene cyanoacetates, and **6** is similar to **3**, but the methyl ester group has been substituted for a phenyl-sulfonyl group. Synthesis of **3** through **6** together with the basic spectroscopic properties is described elsewhere [27].

Determining temperature-dependent viscosity behavior

The viscosity of the various solvents was measured in a Brookfield DV III+ cone-and-plate rheometer with a CP-40 cone and Rheocalc v2.3 software (Brookfield Engineering, Middleboro, MA). A volume of 800 µL of each solvent was placed into the device cup, which was temperature-controlled with circulating water from a temperature-controlled water bath. The temperature in the water bath was continually increased in 3° increments from 15 to 45°C. Temperature inside the rheometer cup was measured with the rheometer's built-in temperature probe. After the temperature stabilized for each 3° increment, viscosity was measured and recorded using the Rheocalc software, which controlled all aspects of testing. Maximum spindle speed was automatically determined to stay below the maximum allowable torque. The viscosity readings at the highest torque and at the two next lower torque settings, both upon ramping up and ramping down, were

averaged to provide one single viscosity value for each temperature step. Equation 9, which is a simplified form of Eq. 6, was fit into the data to obtain the empirical constants A, B, and T_0 for each solvent.

$$\eta(T) = \exp\left(A + \frac{B}{T + T_0}\right) \qquad (9)$$

Measuring fluorescence intensity emission

Stock solutions of the molecular rotors **1** through **6** were created at a concentration of 5 mM in dimethyl sulfoxide (DMSO, fluorscopic grade, Sigma-Aldrich). A 20 μL aliquot of the stock solution was then thoroughly mixed with 10 mL of each solvent to afford a final concentration of 10 μM of the molecular rotor. Out of 48 possible combinations, only CCVJ in dimethylformamide and CCVJ in *n*-methyl-2-pyrrolidone were not examined, because CCVJ precipitates in those solvents. For each sample, 3.5 mL were filled into methacrylate fluoroscopic cuvettes and placed in a Spex Fluoromax-3 Fluorophotometer. Temperature was controlled with a thermoelectrically controlled sample holder (Quantum Northwest Turret-400). After the optimal excitation was found for each sample, a time-based acquisition scan was performed with an integration time of one second. Temperature was increased in increments of 3° from 15° to 45°C every 900 s. Over a time span of 9,900 s, an intensity time-course for each solvent-rotor solution was obtained. Intensity was averaged over 200 s for each plateau after the fluid was allowed to equilibrate for 700 s after each temperature change. The averaged intensity was taken as a single data point of intensity as a function of temperature, $I(T)$.

Statistical tools

All data analysis and graphing, including nonlinear regression, was performed with Graphpad Prism (version

5). Equation 9 was entered as custom equation, and the viscosity data points at their temperature provided the constants A, B, and T_0 for each solvent. From these constants, the viscosity was computed to form a table of matching intensity over viscosity for each solvent-dye combination, finally leading to a table of ζ over T for each solvent-dye combination, which were then plotted. For each data set of $\zeta(T)$, we also computed the mean value $\mu(\zeta)$ and standard deviation $\sigma(\zeta)$, and defined the coefficient of variation $CV(\zeta) = \sigma(\zeta)/\mu(\zeta)$ as a measure of variability. Because of the low number of samples, nonparametric statistical tests were used throughout, notably the Mann–Whitney test to compare two groups and the Kruskal–Wallis test to compare multiple groups.

Results

The Vogel–Fulcher–Tammann model, represented by Eq. 9, described the viscosity data $\eta(T)$ well with $R^2 > 0.998$ in all cases, and data were described significantly (F-test, $P < 0.0001$) better by Eq. 9 than by the Arrhenius model, that is, the empirical form of Eq. 9 with $T_0 = 0$. Two representative results of the nonlinear regression are shown in Fig. 2.

All molecular rotors showed a decrease of their emission intensity as the cuvette temperature was raised. A representative emission timecourse and the resulting data of temperature-dependent intensity, $I(T)$, is shown in Fig. 3. Intensity data $I(T)$ and computed viscosity data $\eta(T)$ were now combined through Eq. 8 under the assumption of a constant exponent $x = 0.6$ (a value frequently used in the literature). The result was the apparent intrinsic temperature-dependency of the molecular rotor in its respective solvent.

We found no uniform trend of $\zeta(T)$ in dependency of the temperature T. Some molecular rotors (notably **1** and **4**) show very low variability of $\zeta(T)$. Some

Fig. 2 Measured viscosity as a function of temperature, illustrated with the example of ethanol (**a**) and pentanol (**b**). The data were fitted using the Vogel–Fulcher–Tammann model, Eq. 9
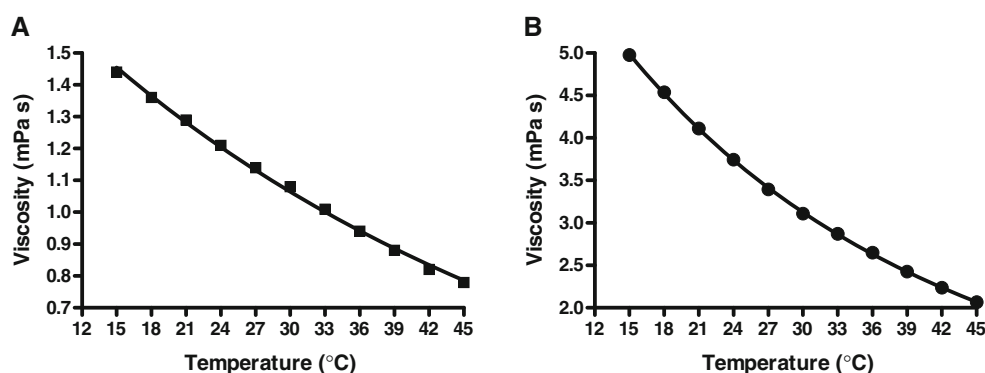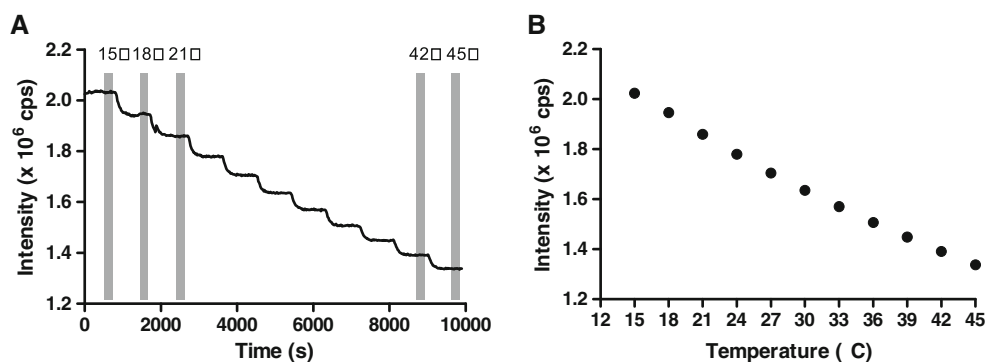
Fig. 3 Intensity time-course of DCVJ **1** dissolved in ethanol (**a**) shown as one representative example. The intensity was averaged for 200 samples (200 s) before the next temperature step as indicated by *gray bars* for the first and last temperature steps. After each temperature step, the fluid temperature was allowed to equilibrate for 700 s. Eleven average intensity values were computed from each timecourse and drawn over the temperature (**b**)

Fig. 4 Intrinsic intensity $\zeta(T)$ as a function of temperature for molecular rotors **1**–**6** in all solvents. CCVJ (**2**) was not examined in dimethylformamide and *n*-methyl-2-pyrrolidone due to poor solubility. Many rotor-solvent combinations, for example, **1** in all solvents, show a low variability of $\zeta(T)$ with the temperature. Although some combinations (e.g., **2** or **6** in ethylene glycol) show a decrease of the intrinsic intensity with temperature and would show good empirical fit with Eq. 3, combinations can be found where the calculated $\zeta(T)$ increases with temperature (e.g., **3** in DMSO, **6** in dimethylformamide) or even exhibits a u-shape with an apparent preferential temperature that minimizes $\zeta(T)$ (e.g., **2** in ethanol, **4** in dimethylformamide)
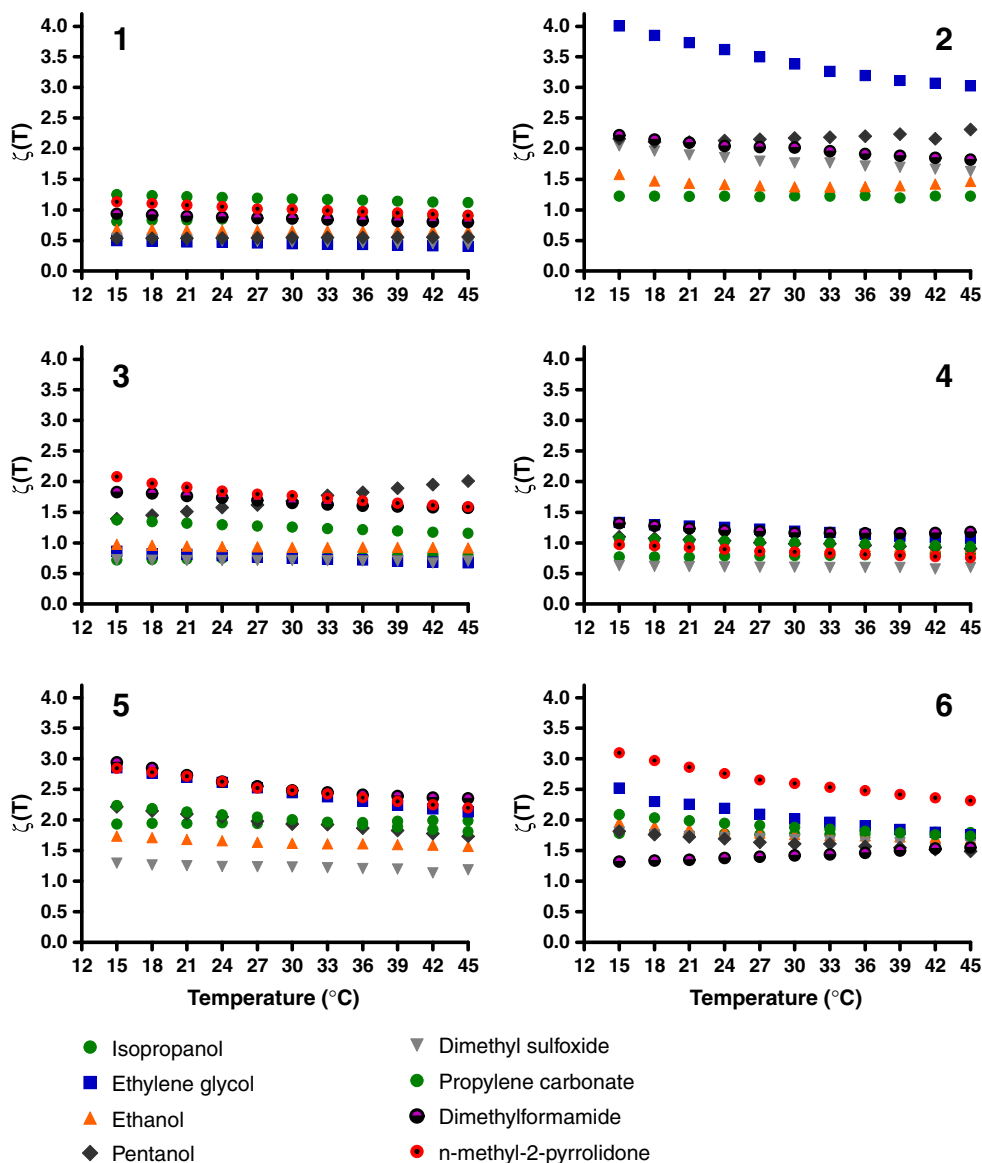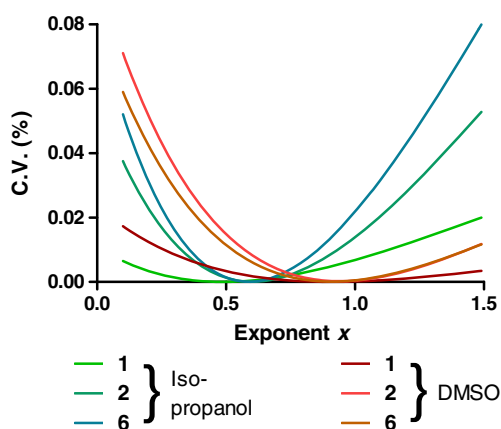
Fig. 5 Coefficient of variation C.V. of $\zeta(T)$ with changing exponent x. Shown are three representative dyes (**1** with low polarity, **2** and **6** with some polarity) in isopropanol and DMSO. For each combination of dye and solvent, a specific value of x exists that minimizes the coefficient of variation. The value of x is closer to unity in the polar aprotic solvent DMSO than in the polar protic solvent isopropanol

combinations, foremost **2** in ethylene glycol, **3**, **5**, and **6** in *n*-methyl-2-pyrrolidone, show a decrease of the intrinsic intensity with temperature, which could be well described by the Arrhenius model (Eq. 3). On the other hand, several combinations show an increasing trend of $\zeta(T)$, for example, **2** in pentanol, **6** in dimethylformamide, and **3** in DMSO. Furthermore, in several instances, u-shaped curves of $\zeta(T)$ over T can be seen, most notably **2** in ethanol and pentanol, and **4** in dimethylformamide. The plots of $\zeta(T)$ over T for all possible rotor-solvent combinations and under the assumption of a constant $x = 0.6$ can be seen in Fig. 4.

The non-uniform trend of $\zeta(T)$ over T and the low variability of $\zeta(T)$ in some cases led us to the question

whether the assumption of $x = 0.6$ is valid. Using the exact value $x = 2/3$ found by Förster and Hoffmann [14] did not fundamentally change the trends we found (data not shown). We now examined whether a value of x existed that minimized the variability of $\zeta(T)$ with the temperature. Computation of $CV(\zeta)$ as a function of x revealed a distinct minimum in all cases. The variation of $CV(\zeta)$ with the exponent x is shown in Fig. 5 in two representative solvents and three representative dyes. In all dye-solvent combinations, one specific value of x exists, where the coefficient of variation becomes very small. We refer to this value of x as the "optimal" x. The optimal x is higher in the less-polar solvents than in the polar-protic group. Averaged over all dyes, the mean value of the optimal x is 0.68 for the polar protic solvents (isopropanol, ethylene glycol, ethanol, and pentanol) compared to 0.98 for the aprotic solvents (DMSO, DMF, NMP, and propylene carbonate). The difference is statistically significant (Mann–Whitney test, $P < 0.0001$). Furthermore, the mean value for the polar protic solvents (0.68) is very close to the theoretical value (2/3) predicted by Förster and Hoffmann [14]. One notable exception is dye **6** in DMF, where the optimal x of 0.43 is the smallest value encountered. Finally, a very weak trend exists that the optimal x increases with the number of carbons in the anilino group of dyes **3**, **4**, and **5**. A linear trend between the number of carbons and x is only statistically significant for isopropanol. However, the optimal x value is higher for **5** than for **3** in all solvents (average: 10%, range 1.8–16.3%, statistically significant difference from zero with the Wilcoxon signed rank test, $P < 0.008$). Table 1 shows the optimal x values and the corresponding values of ζ, averaged over the entire temperature range, for all solvent-dye combinations. Note that ζ has units of 10^6 counts per second because of the instrument gain factor G (Eq. 4).

Table 1 Summary of the optimal x values and the corresponding values of ζ, averaged over the entire temperature range, for all dye-solvent combinations

Dye	Optimal x						Average ζ (x10^6 cps)					
	1	**2**	**3**	**4**	**5**	**6**	**1**	**2**	**3**	**4**	**5**	**6**
Isopropanol	0.50	0.60	0.59	0.49	0.52	0.57	0.38	1.22	1.79	0.76	0.83	1.99
Ethylene glycol	0.77	0.83	0.88	0.79	0.78	0.84	0.29	1.86	0.98	0.46	0.74	1.31
Ethanol	0.67	0.69	0.81	0.68	0.72	0.75	0.66	1.42	1.77	0.93	0.94	1.62
Pentanol	0.56	0.52	0.75	0.65	0.66	0.71	0.57	2.18	1.41	0.67	0.56	1.08
DMSO	0.91	0.94	0.92	0.88	0.90	0.98	0.39	1.43	1.31	1.05	0.81	1.51
DMF	1.10	–	0.43	1.10	0.93	1.20	0.93	–	1.57	1.81	1.26	2.79
Propylene carbonate	0.78	0.91	0.90	0.88	0.80	0.94	1.02	1.55	1.48	1.00	0.85	1.52
NMP	1.00	–	1.20	1.10	1.10	1.10	0.83	–	1.95	1.39	0.67	1.94

Discussion

Molecular rotors have recently gained popularity as nonmechanical viscosity probes for bulk fluids [19, 28, 29] and as microviscosity probes in liposomes [7, 30–32] and cells [13, 17, 20, 21]. In many environments, the temperature can be controlled, and the observation of relative changes of viscosity is possible. If two intensity measurements I_1 and I_2 are taken at a constant temperature, for example, before and after the application of a viscosity-altering treatment, the ratio of two emissions (cf. Eq. 5) becomes:

$$\frac{I_1}{I_2} = \frac{G \cdot \hat{C}(T) \cdot \eta_1^x}{G \cdot \hat{C}(T) \cdot \eta_2^x} = \left(\frac{\eta_1}{\eta_2}\right)^x \qquad (10)$$

where η_1 and η_2 are the viscosities before and after treatment, respectively (see, e.g., [17, 32, 33]). The constants G and $\hat{C}$ cancel out under identical experimental conditions, most importantly, identical dye concentration, constant temperature and constant excitation intensity. If the viscosity before treatment (η_1) is known, Eq. 10 can be solved for the unknown η_2:

$$\eta_2 = \eta_1 \cdot \left(\frac{I_2}{I_1}\right)^{\frac{1}{x}} \qquad (11)$$

However, this approach requires that the constant x is known. Furthermore, if absolute measurements are required, the additional proportionality constants G and $\hat{C}$ need to be determined as well. Moreover, a temperature-dependent behavior of the dye constants (namely, $\hat{C}$), influences the ability of molecular rotors to measure viscosity. Since all fluids exhibit decreasing viscosity with increasing temperature, a molecular rotor in solution is expected to show a reduced quantum yield to reflect the reduced solvent viscosity. When the quantum yield is directly influenced by the temperature, however, viscosity measurement becomes more complex, because the intrinsic temperature-dependency needs to be accounted for. Notably, if η_1 and η_2 in Eq. 10 are taken at different temperatures, $\hat{C}(T)$ in the numerator and denominator cancel out only if they are temperature-independent.

The original goal of this study was to determine the temperature behavior of the intrinsic quantum yield $\hat{C}$. Under the original hypothesis, the intrinsic reorientation rate is a thermally-induced process [3, 18, 30], and therefore the intrinsic quantum yield was expected to decrease with temperature. Our results do not support this hypothesis. Rather, we found that the emission intensity decrease in solvents of increasing temperature

was fully explained by the decreasing viscosity of the solvent, provided that the exponent x of the Förster–Hoffmann equation (Eq. 1) is seen as dependent on both the dye and the solvent. Under the assumption of a constant (that is, solvent-independent) exponent x, the intrinsic quantum yield $\hat{C}$ shows variability with temperature. However, we did not find uniform behavior of $\hat{C}$ with temperature. Among the possible functions $\hat{C}(T)$, e.g., exponentially decreasing or linearly increasing, the instances where we found u-shaped functions with an apparent preferential temperature convinced us that no universal model exists that explained our measured $\hat{C}(T)$.

Under a modified hypothesis we now assumed that $\hat{C}(T) = $ const, whereby the exponent x now becomes part of the nonlinear regression process to fit the function in Eq. 1 into our intensity/temperature data. We found that Eq. 1 can indeed explain the measured data for $\hat{C}(T) = $ const, but that x now depends on the dye and the solvent, with a noticeable increase of x in aprotic solvents.

Polar protic solvents (in this study, isopropanol, ethylene glycol, ethanol and pentanol) possess an acidic hydrogen and can therefore display hydrogen bonding in addition to polar-polar interaction with the dye. On the other hand, polar aprotic solvents (in this study, DMSO, DMF, propylene carbonate and n-methyl-2-pyrrolidone) do not possess an acidic hydrogen and do not display hydrogen bonding. In accordance with the literature (see, e.g., [1, 5, 34]) we interpret the intensity data in this study as a consequence of three competing mechanisms that influence the formation rate of TICT states: Solvent viscosity, which hinders TICT formation through microfriction, polar-polar interaction and hydrogen bonding, which both stabilize the TICT states [35–38].

Polar–polar interaction can be quantified through the dipole moment, which causes the solvent molecules to reorient around the excited-state fluorophore, or through the dielectric constant. However, we found no statistical correlation between the optimum x and either the dipole moment or the dielectric constant (Table 2). For this reason, we conclude that the ability to form hydrogen bonds primarily influences the exponent in Eq. 1. Solvents unable to form hydrogen bonds lead to values of x closer to unity, whereas the presence of bond-forming hydrogen atoms leads to a lower value of x. Taking this idea to the extreme, we could speculate that the reorientation rate depends linearly on Debye–Stokes–Einstein viscous friction [16] and in a power-law fashion on hydrogen bond formation. The combination

Table 2 Dipole moment and dielectric constants of the eight solvents used in this study [39]

Solvent	Dipole moment (Debye)	Dielectric constant
Isopropanol	1.66	18.2
Ethylene glycol	2.36	41.4
Ethanol	1.69	25.3
Pentanol	1.70	15.1
DMSO	3.96	46.5
DMF	3.82	37.1
Propylene carbonate	4.97	65.1
NMP	0.57	32.2

of both effects would lead to a form of Eq. 1, because hydrogen bond formation would dominate at low viscosities, whereas viscous microfriction would dominate at high viscosities. However, we are unable to directly support this speculation with our data, and due to the extremely poor solubility of the molecular rotors in nonpolar solvents, such experiments would be difficult to conduct.

The constant ζ (second half of Table 1) describes the intrinsic quantum yield $\hat{C}$ of each dye, multiplied with the instrument gain G that we assume to be constant throughout the study. Therefore, ζ is a dye- and solvent-dependent constant that is independent of the solvent viscosity. With the exception of CCVJ, where two data points are missing due to poor solubility, ζ is higher in average in the polar aprotic solvents than in the polar protic solvents. This observation is consistent with the notion that hydrogen bond formation stabilizes the TICT state and therefore enhances the TICT formation rate [35–38]. However, the differences between the values of ζ in protic and aprotic solvents are statistically not significant (Kruskal–Wallis test with Dunns multiple comparison test) and may be attributed to experimental error, to the relatively low number of solvents analyzed and to the high variability of the ζ-values within each solvent group.

In conclusion, we separated extrinsic influences (i.e., solvent viscosity) and intrinsic influences (i.e., solvent-independent TICT formation rate) of the temperature on the emission intensity, and thus the quantum yield, of viscosity-sensitive molecular rotors. We found that the intensity changes are fully explained by the temperature-dependent changes of solvent viscosity. Our conclusion is that the TICT formation rate is governed by solvent polarity, viscosity, and its ability to form hydrogen bonds, but temperature does not influence the TICT formation rate directly in a measurable way. The results of this study support the application of molecular rotors as viscosity sensors in environments of variable temperature. However, we also found that the quantitative measurement of the solvent viscosity requires the individual calibration (that is, the determination of the constants $\hat{C}$ and x) for the individual solvent type.

Which of the molecules examined in this study would be the optimum viscosity sensor? The choice of a suitable molecule is dominated by the application, for example, whether a hydrophobic or more hydrophilic molecule, such as **2**, is desired. From their photophysical behavior, a choice can be made by comparing the exponent x, which can be interpreted as the molecular rotor's sensitivity to viscosity changes (Eq. 11), or the intrinsic quantum yield $\hat{C}$, which can be seen as the molecular rotor's viscosity-independent base intensity (Eq. 5). Compound **3** has the highest value of x in most polar solvents (Table 1) and can be considered a good choice for high sensitivity, followed by **6**, which has higher x-values in aprotic solvents. In applications where a low concentration of dye is required, a high value of $\hat{C}$ (and correspondingly, ζ) is desirable. Both **2** and **6** can be noted for their brightness, which is also reflected by high values of ζ in Table 1.

References

1. Law KY (1980) Fluorescence probe for microenvironments: anomalous viscosity dependence of the fluorescence quantum yield of pn, n-dialkylaminobenzylidenemalononitrile in 1-alkanols. Chem Phys Lett 75(3):545–549
2. Loutfy RO, Law KY (1980) Electrochemistry and spectroscopy of intramolecular charge-transfer complexes. pn, n-dialkylaminobenzylidenemalonitriles. J Phys Chem 84:2803–2808
3. Safarzadeh-Amiri A (1986) Solvent and temperature effects on the decay dynamics of [pn, n-(dialkylamino) benzylidene] malononitriles. Chem Phys Lett 129(3):225–230
4. Haidekker MA, Theodorakis EA (2007) Molecular rotors fluorescent biosensors for viscosity and flow. Org Biomol Chem 5(11):1669–1678
5. Grabowski ZR, Rotkiewicz K, Rettig W (2003) Structural changes accompanying intramolecular electron transfer: focus on twisted intramolecular charge-transfer states and structures. Chem Rev (Columbus) 103(10):3899–4032
6. Allen BD, Benniston AC, Harriman A, Rostron SA, Yu C (2005) The photophysical properties of a julolidine-based molecular rotor. Phys Chem Chem Phys 7(16):3035–3040
7. Kung CE, Reed JK (1986) Microviscosity measurements of phospholipid bilayers using fluorescent dyes that undergo torsional relaxation. Biochemistry 25(20):6114–6121
8. Haidekker MA, Brady TP, Lichlyter D, Theodorakis EA (2005) Effects of solvent polarity and solvent viscosity on the fluorescent properties of molecular rotors and related probes. Bioorganic Chem 33(6):415–425

9. Loutfy RO (1986) Fluorescence probes for polymer free-volume. NATO ASI Ser, Ser C: Math Phys Sci 182:429–448

10. Iwaki T, Torigoe C, Noji M, Nakanishi M (1993) Antibodies for fluorescent molecular rotors. Biochemistry 32(29):7589–7592

11. Viriot ML (1998) Molecular rotors as fluorescent probes for biological studies. Clin Hemorheol Microcirc 19(2):151–160

12. Ghiggino KP, Hutchison JA, Langford SJ, Latter MJ, Lee MA, Lowenstern PR, Scholes C, Takezaki M, Wilman BE (2007) Porphyrin-based molecular rotors as fluorescent probes of nanoscale environments. Adv Funct Mater 17(5):805

13. Kuimova MK, Yahioglu G, Levitt JA, Suhling K (2008) Molecular rotor measures viscosity of live cells via fluorescence lifetime imaging. J Am Chem Soc 130(21):6672–6673

14. Förster T, Hoffmann G (1971) Die viskositätsabhngigkeit der fluoreszenzquantenausbeuten einiger farbstoffsysteme (effect of viscosity on the fluorescence quantum yield of some dye systems). Z Phys Chem 75:63–76

15. Loutfy RO, Arnold BA (1982) Effect of viscosity and temperature on torsional relaxation of molecular rotors. J Phys Chem 86(21):4205–4211

16. Haidekker M, Theodorakis E (2010) Environment-sensitive behavior of fluorescent molecular rotors. J Biol Eng 4:11

17. Haidekker MA, L'Heureux N, Frangos JA (2000) Fluid shear stress increases membrane fluidity in endothelial cells: a study with dcvj fluorescence. Am J Physiol Heart Circ Physiol 278(4):H1401

18. Vogel M, Rettig W (1987) Excited state dynamics of triphenylmethane-dyes used for investigation of microviscosity effects. Ber Bunsenges Phys Chem 91(11):1241–1247

19. Haidekker MA, Tsai AG, Brady T, Stevens HY, Frangos JA, Theodorakis E, Intaglietta M (2002) A novel approach to blood plasma viscosity measurement using fluorescent molecular rotors. Am J Physiol Heart Circ Physiol 282(5):1609–1614

20. Kuimova MK, Botchway SW, Parker AW, Balaz M, Collins HA, Anderson HL, Suhling K, Ogilby PR (2009) Imaging intracellular viscosity of a single cell during photoinduced cell death. Nat Chem 1(1):69–73

21. Luby-Phelps K, Mujumdar S, Mujumdar RB, Ernst LA, Galbraith W, Waggoner AS (1993) A novel fluorescence ratiometric method confirms the low solvent viscosity of the cytoplasm. Biophys J 65(1):236–242

22. Vogel H (1921) The law of the relation between the viscosity of liquids and the temperature. Phys Z 22:645–646

23. Fulcher GS (1925) Analysis of recent measurements of the viscosity of glasses. J Am Ceram Soc 8(6):339–355

24. Tammann G, Hesse W (1926) Temperature dependence of viscosity of melted supercooled liquids. Z Anorg Allg Chem 156:245–247

25. Hui H, Zhang Y (2007) Toward a general viscosity equation for natural anhydrous and hydrous silicate melts. Geochim Cosmochim Acta 71(2):403–416

26. Kivelson D, Tarjus G, Zhao X, Kivelson SA (1996) Fitting of viscosity: Distinguishing the temperature dependences predicted by various models of supercooled liquids. Phys Rev E 53(1):751

27. Sutharsan J, Lichlyter D, Wright N, Dakanali M, Haidekker M, Theodorakis E (2010) Molecular rotors: synthesis and evaluation as viscosity sensors. Tetrahedron 66:2582–2588

28. Akers WJ, Haidekker MA (2004) A molecular rotor as viscosity sensor in aqueous colloid solutions. J Biomech Eng 126:340

29. Akers WJ, Haidekker MA (2005) Precision assessment of biofluid viscosity measurements using molecular rotors. J Biomech Eng 127:450–454

30. Lukac S (1984) Thermally induced variations in polarity and microviscosity of phospholipid and surfactant vesicles monitored with a probe forming an intramolecular charge-transfer complex. J Am Chem Soc 106(16):4386–4392

31. Furuno T, Isoda R, Inagaki K, Iwaki T, Noji M, Nakanishi M (1992) A fluorescent molecular rotor probes the kinetic process of degranulation of mast cells. Immunol Lett 33(3):285–288

32. Nipper ME, Majd S, Mayer M, Lee JCM, Theodorakis EA, Haidekker MA (2008) Characterization of changes in the viscosity of lipid membranes with the molecular rotor fcvj. BBA-Biomembranes 1778(4):1148–1153

33. Mallipattu S, Haidekker M, Von Dassow P, Latz M, Frangos J (2002) Evidence for shear-induced increase in membrane fluidity in the dinoflagellate lingulodinium polyedrum. J Comp Physiol A 188(5):409–416

34. Haidekker M, Nipper M, Mustafic A, Lichlyter D, Dakanali M, Theodorakis E (2010) Advanced fluorescence reporters in chemistry and biology I: fundamentals and molecular design, chap. In: Dyes with segmental mobility: molecular rotors. Springer, New York, pp 267–308

35. Wehry E (1990) Practical fluorescence, chap. In: Effects of molecular environment on fluorescence and phosphorescence. Marcel Dekker, New York

36. Schuddeboom W, Jonker SA, Warman JM, Leinhos U, Kühnle W, Zachariasse KA (1992) Excited-state dipole moments of dual fluorescent 4-(dialkylamino) benzonitriles. Influence of alkyl chain length and effective solvent polarity. J Phys Chem 96:10809–10819

37. Kim YH, Cho DW, Yoon M, Kim D (1996) Observation of hydrogen-bonding effects on twisted intramolecular charge transfer of p-(n, n-diethylamino) benzoic acid in aqueous cyclodextrin solutions. J Phys Chem 100(39):15670–15676

38. Bangal PR, Panja S, Chakravorti S (2001) Excited state photodynamics of 4-n, n-dimethylamino cinnamaldehyde: a solvent dependent competition of tict and intermolecular hydrogen bonding. J Photochem Photobiol, A Chem 139(1):5–16

39. Haynes W (2010) CRC handbook of chemistry and physics, 91st edn. CRC Press, Boca Raton